

# YingLong: Skillful High Resolution Regional Short Term Forecasting with Boundary Smoothing

Pengbo Xu,<sup>1,2</sup> Tianyan Gao,<sup>3</sup> Yu Wang,<sup>3</sup> Junping Yin,<sup>4,5,2,\*</sup> Juan Zhang,<sup>6,2</sup>  
Xiaogu Zheng,<sup>2,7</sup> Zhimin Zhang,<sup>8</sup> Xiaoguang Hu,<sup>8</sup> and Xiaoxu Chen<sup>8</sup>

<sup>1</sup>*School of Mathematical Sciences, Key Laboratory of MEA (Ministry of Education),  
Shanghai Key Laboratory of PMMP, East China Normal University, Shanghai 200241, P.R. China.*

<sup>2</sup>*Shanghai Zhangjiang Institute of Mathematics, Shanghai, 201203, P.R. China.*

<sup>3</sup>*School of Mathematics and Statistics, Northeast Normal University, Changchun 130000, P.R. China*

<sup>4</sup>*Institute of Applied Physics and Computational Mathematics, Beijing, 100094, China.*

<sup>5</sup>*National Key Laboratory of Computational Physics, Beijing 100088, China.*

<sup>6</sup>*Institute of Artificial Intelligence, Beihang University, Beijing, 100191, China.*

<sup>7</sup>*International Global Change Institute, Hamilton, New Zealand.*

<sup>8</sup>*Baidu Inc., Beijing, China, 100085.*

(Dated: January 30, 2024)

In the realm of numerical weather forecasting, achieving higher resolution demands increased computational resources and time investment, and leveraging deep learning networks trained solely on data significantly reduces the time expenditure during forecasting. Recently, several global forecasting artificial-intelligence-based models are developed, which are mainly trained on reanalysis dataset with a spatial resolution of approximately 25km. However, regional forecasting prefers a higher spatial resolution, and boundary information for the region also plays an important role in regional forecasting, which turns out to be a major difference from global forecasting. Here we introduce a high-resolution, short-term regional weather forecasting, artificial-intelligence-based model called “YingLong”, which is capable of hourly predicting weather fields including wind speed, temperature, and specific humidity at a 3km resolution. YingLong utilizes a parallel structure of global and local blocks to capture multiscale meteorological features and is trained on analysis dataset. Additionally, the necessary information around the regional boundary is introduced to YingLong through the boundary smoothing strategy, which significantly improves the regional forecasting results. By comparing forecast results with those from WRF-ARW, one of the best numerical prediction models, YingLong demonstrates superior forecasting performances in most cases, especially on surface variables.

## I. INTRODUCTION

In recent years, due to global climate change, the frequency of extreme weather events increases year by year, leading to serious meteorological disasters and having a serious impact on human production and life. Accurate weather forecasting plays a crucial role in various aspects of modern society [1]. Over the past decades, the research field of numerical weather prediction (NWP) has seen rapid development [2, 3]. Currently, weather forecasts primarily rely on NWP models for the periodic release of results. Traditional NWP models primarily follow a simulation-based paradigm, transforming the physical laws governing atmospheric states into partial differential equations (PDEs) and then employing numerical simulation methods for solution [4, 5]. Due to the complexity of solving PDEs, these NWP models typically run quite slowly [6–8]. Additionally, traditional NWP models heavily rely on parametric numerical models [9], which are often considered to be incomplete and prone to errors [10, 11].

Recently, with the development of deep learning, more and more researchers become increasingly interested

in artificial intelligence (AI)-based weather forecasting models [12–19]. The AI-based model FourCastNet [20] generates a global weather forecast for the first time at a spatial resolution of  $0.25^\circ \times 0.25^\circ$  (approximately  $25\text{km} \times 25\text{km}$ ), matching the ECMWF Integrated Forecasting System (IFS) [21]. FourCastNet marks the first direct comparison between deep learning weather models and the traditional NWP model. Afterward, there are an abundance of research achievements trained on the ERA5 [22] dataset, including Pangu-Weather [23] which surpasses in accuracy and speed over IFS for the first time, GraphCast [24], FengWu [25], FuXi [26], and ClimateX [27]. However, when forecasting small-scale weather phenomena and extreme weather events, the resolution of  $0.25^\circ$  is always insufficient. Such as a spatial resolution of 3 km can effectively describe the mesoscale convective structure associated with mid latitude squall line systems [28]. In operational forecasting, analysis data is usually preferred to be utilized as the initial condition for the NWP model rather than reanalysis data. And AI-based models, MetNet2 [29] and MetNet3 [30], use the higher spatial resolution analysis data in training. Moreover, the MetNet series focuses more on forecasting precipitation and some individual meteorological variables rather than a complete meteorological field forecast. And MetNet2 and MetNet3 primarily forecast radar, satellite and ground observation station data, utilizing analysis data

---

\* yinjp829829@126.com

only to improve the model training, not as forecast results [31].

To address the void in AI-based weather forecasting regional models at high resolutions  $3\text{km} \times 3\text{km}$ , we propose our YingLong model. The main contributions of this paper are listed in the following two aspects. First, to address the multiscale problem, we employ a parallel network architecture integrating AFNO [32] and Swin transformer block [33]. The Swin transformer block excels at extracting local spatial features, while AFNO excels at capturing global spatial features. Our parallel structure effectively combines their advantages, enabling the extraction of both local and global features at the same time. Second, during inference, we utilize the boundary smoothing strategy, which turns out to be crucial to regional forecasting. We forecast the future state of 69 variables for the next 12 hours and quantify the skillfulness of YingLong models with different numbers of layers and the NWP model against analysis data. For the majority of cases on surface variables or upper-air variables, YingLong makes better predictions than the NWP model utilized in the HRRR dataset, which is WRF-ARW. YingLong demonstrates a notable advantage in forecasting near-surface variables. For example, in the forecast for variable U10 (u-component of 10m wind), YingLong exhibited around 19% decrease in RMSE compared to NWP. For upper-air variables, YingLong also exceeds NWP in forecasting multiple variables across various pressure levels.

## II. REGIONAL WEATHER FORECASTING WITH BOUNDARY SMOOTHING

For training and evaluating the YingLong model, we choose to utilize the analysis subset of the High-Resolution Rapid Refresh (HRRR) dataset [34], which is generated through the Gridpoint Statistical Interpolation analysis system (GSI). Besides, the HRRR dataset also provides forecast results obtained from NWP, which is generated through the Advanced Research version of the Weather Research and Forecasting Model (WRF-ARW). Both the analysis and NWP results of the HRRR dataset are hourly updated at 3-km grid resolution and operated by the National Oceanic and Atmospheric Administration (NOAA), covering the CONUS and Alaska with multiple variables. We select the southeastern region of the United States shown in Fig. 1(a), which is around the range of 110-130E, 15-35N, with  $440 \times 408$  grid points in Lambert projection. The YingLong model takes the analysis data at some given time point, and gives the forecasting results at a future time point with a lead time of 1 hour. Then the supervised learning is utilized by choosing the analysis results at the corresponding future time point as labels. The training dataset ranges from 2015 to 2021, and the data in 2022 is for testing.

The architecture for the YingLong model is shown in Fig. 1(b). At present, many famous deep learning

weather forecast models are based on the Vision Transformer (ViT) backbone [35], such as Pangu-Weather [23], FourCastNet [20], where the former one uses Shift window transformer block (Swin) [33] and the latter one uses Adaptive Fourier Neural Operator (AFNO) [32] as their core modules, respectively. In this work, since we deal with a 3km regional grid, the large and medium spatial scales also play important roles in short term forecasting. Therefore, YingLong captures various features of variables at different scales. In order to deal with the multiscale problem, we utilize the Window Multi-head Self-Attention (W-MSA), and Shift Window Multi-head Self-Attention (SW-MSA) blocks in Swin Transformer [33] to capture the local features of different variables, as shown in Fig. 1(c). Besides, the AFNO block mainly captures the global features of the variables at the target region from the Fourier frequency space, which can also be found in Fig. 1(c). After learning local and global features separately, the YingLong model also combines these multiscale features together. In this paper we mainly choose 12 layers (YingLong-12) and 24 layers (YingLong-24). The complete training process for YingLong-12 requires approximately 80 hours using 8 Nvidia V100 GPUs, and YingLong-24 requires approximately 253 hours using 8 Nvidia P40 GPUs.

In the inference stage, the involving of proper information around the regional boundary is quite important for the weather forecasting on the local region, since the weather conditions over the outside region effect more and more on the variables within the region; otherwise, the deep learning model should give an inference based on little information, which is a quite heavy task for the AI-based model. For the convenience of consideration, the region shown in Fig. 1(a) is divided into two parts, the interior part (the pink area in Fig. 1(a)) and the transition part (the yellow area in Fig. 1(a)) which is a band between the external region and interior part. Length of the transition zone is 207 km empirically, which consists of 69 grid points. Within the transition part, a boundary smoothing strategy is utilized, which is an average of YingLong with weight  $\alpha$  and the NWP model with weight  $1 - \alpha$ . From the outer boundary to the inner boundary,  $\alpha$  transits from 0 to 1, as shown in Fig. 1(a). Then the boundary smoothing results can be the input for the next step of YingLong forecasting.

## III. EXPERIMENTAL SETTINGS

We mainly trained two YingLong models with different numbers of layers on the HRRR dataset, and the following experiment results indicate that each model has its own advantage. The first model, YingLong-12, mainly considers 24 variables, including 4 surface variables and 20 upper-air variables distributed at 4 pressure levels (50hpa, 500hpa, 850hpa, 1000hpa). And the other model, YingLong-24, mainly considers 69 variables, including the 24 variables utilized in YingLong-12,

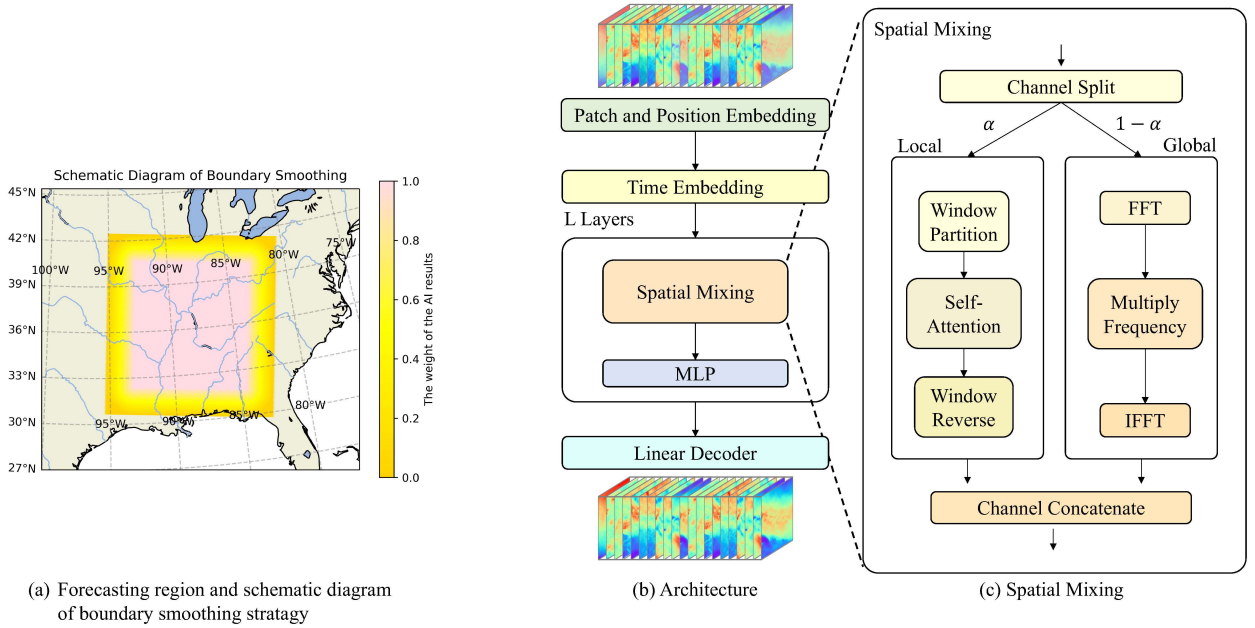


FIG. 1. Boundary smoothing strategy and architecture for the YingLong model. (a), the colored area is the forecasting region, the yellow or pink indicating weight of YingLong forecasting results, and the weighted average of YingLong and NWP results, which is boundary smoothing. (b), the architecture for the YingLong model, where the spatial mixing block is shown in (c). The design of the architecture is inspired by Swin to capture the local features and AFNO to capture the global features of variables.

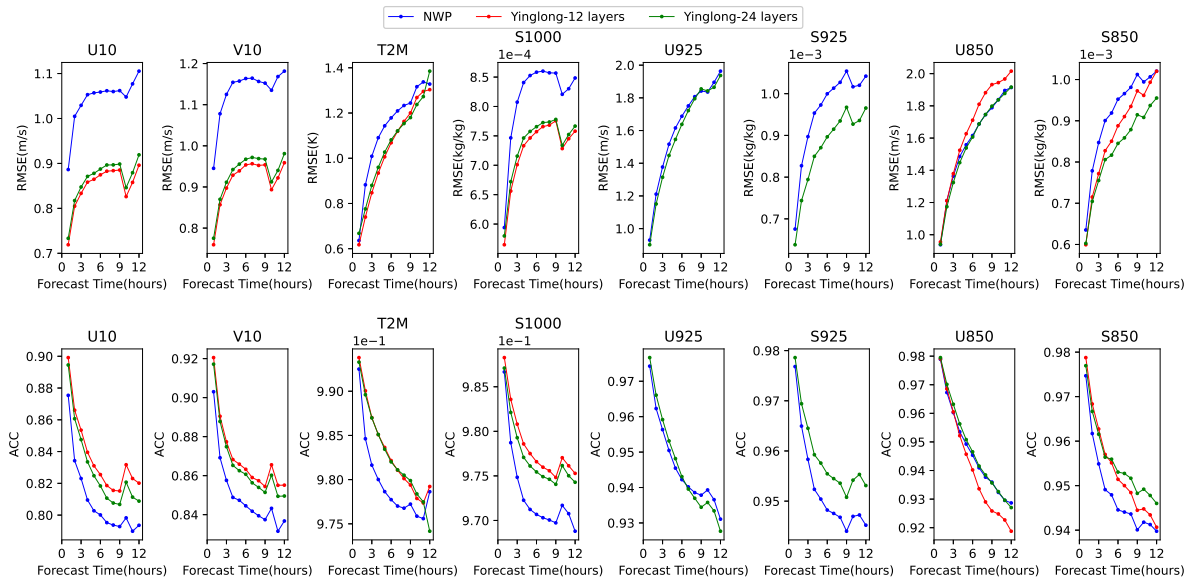


FIG. 2. The RMSEs (where the lower values are preferred) and ACCs (where the higher values are preferred) of the forecasting results from the YingLong and NWP models (i.e., WRF-ARW). Among the variables, T2M represents the 2-meter temperature, U10 and V10, respectively, represent the u-component and v-component of the 10-meter wind speed, and S1000 represents the specific humidity at 1000hPa. U925, S925, U850, and S850 represent the u-component of the wind speed and specific humidity at 925hPa and 850hPa, respectively.

and the other 45 variables at 9 additional pressure levels (100hPa, 150hPa, 200hPa, 250hPa, 300hPa, 400hPa, 600hPa, 700hPa, and 925hPa). To quantify the skills of the YingLong-12, YingLong-24, and NWP models, we utilized two widely used metrics: root mean square error (RMSE) and anomaly correlation coefficient (ACC). The higher ACC and lower RMSE stand for the better forecasting ability of the corresponding model. We test YingLong-12 and YingLong-24 by utilizing the data in 2022 provided by HRRR. In this part, we set 00:00 (UTC) each day as the initial forecast time for the YingLong model and the lead time  $\Delta t = 1$  hour. By utilizing the boundary smoothing strategy, the forecasting results for each variable for the next twelve hours can be generated. By setting analysis data for the corresponding variable at the same time as the ground truth, we can compare the values of ACC and RMSE obtained from AI-based YingLong-12 and YingLong-24 models and the NWP method, respectively.

## IV. SKILL OF YINGLONG

### A. Surface variables.

For the surface variables, including U10 (u-component of 10m wind speed), V10 (v-component of 10m wind speed), T2M (2m temperature), and S1000 (specific humidity at 1000hpa pressure level), it can be concluded from Fig. 2 that both YingLong-12 and YingLong-24 significantly outperform the NWP method utilized in the HRRR dataset, which is WRF-ARW. Specifically, for the U10 variable, the RMSEs (in m/s) of 12-hour forecasting are 1.106 for NWP, and YingLong-24 and YingLong-12 can reduce it to 0.919 and 0.896, respectively. Comparing with the NWP results, the relative drops of RMSEs are 16.91% and 18.99% for YingLong-24 and YingLong-12, respectively. From the detailed comparison results of U10 and V10 (supplementary materials Table A5), we can conclude that for the short term forecasting, both YingLong models perform significantly more accurate than NWP (i.e., WRF-ARW), further YingLong-12 slightly surpasses YingLong-24.

As for variable T2M, the RMSEs (in K) of NWP at 7h and 12h forecast time are 1.209 and 1.328, respectively. And YingLong-24 generates forecasting results with RMSEs of 1.121 at 7h forecast time and 1.3852 at 12 forecast time, while YingLong-12 drops the RMSE to 1.119 at 7h forecast time and 1.303 at 12h forecast time. Therefore, by comparing with the corresponding NWP results, the relative drops of RMSEs which are 7.30% for YingLong-24 and 7.44% for YingLong-12 at forecast time 7h and 1.81% for YingLong-12 at forecast time 12h indicate that YingLong-12 can give a better forecast result than NWP during the whole twelve-hour forecast time. And from 3h to 8h the improvements of YingLong-12 are more significant. Comparing with YingLong-24, YingLong-12 gives the forecast results of T2M with almost the same RMSE

up to 11h forecast time, while at 12h, YingLong-12 significantly surpasses YingLong-24.

Moreover, the forecasting results of variable S1000 give similar conclusions. Comparing with NWP forecasting results at 7h, the RMSEs are relative drop 10.18% for YingLong-12 and 10.97% for YingLong-24, respectively. Finally, for the surface variables, YingLong-12 performs better than YingLong-24 and NWP, and improves significantly for U10 and V10.

We select some cases and visualize the corresponding forecast results generated by YingLong and NWP, so that the advantages of YingLong can be found more clearly. Fig. 3(a)-(i) show the forecasting results of 10-meter wind speed  $\sqrt{U10^2 + V10^2}$ , T2M, and S1000 obtained from the YingLong model and NWP model utilized in HRRR dataset. It can be found that the results from YingLong model in these cases closely align with the ground truth. By calculating the mean absolute error (MAE) for the forecasting results of YingLong and NWP with the ground truth, the corresponding spatial distribution maps of MAE for each variable are shown in Fig. 3(j)-(o), and we can further observe that the YingLong forecast results are obviously superior to those of the NWP. In fact, for some variables, the YingLong model can still give significantly better forecasting results than those from NWP when the forecast time extends to 48h. Fig. 4 displays the forecast results and spatial distribution maps of MAE for 10m wind speeds (m/s) at 17:00 (UTC) on November 10, 2022, as predicted by the YingLong model and NWP model at 00:00 (UTC) on the same day. The results generated by the YingLong model outperform those of the NWP significantly, which can be found evidently in the spatial distribution map of MAE.

### B. Upper-air variables.

In order to compare the forecast skills of YingLong models with different layers, we further choose some upper-level variables, including U850 (u-component of wind speed at 850hpa), V850 (v-component of wind speed at 850hpa), T850 (temperature at 850hpa) and S850 (specific humidity at 850hpa). The results of RMSE and ACC are shown in supplementary materials Fig. 2 (The results of V850 and T850 are shown in Fig. 6). For the variable U850, RMSEs (in m/s) of NWP, YingLong-12, and YingLong-24 at 12h forecast time are 1.914, 2.016, and 1.916. YingLong-24 gives the forecast results with almost the same RMSE as the results obtained by NWP. And YingLong-24 surpasses YingLong-12 significantly for the variable U850. Similar conclusions can also be obtained for the variables V850 and T850. Further for the variable S850, the corresponding RMSE of NWP at 12h forecast time is  $1.020 \times 10^{-3}$ , while the RMSE of YingLong-24 at the same forecast time drops to  $9.552 \times 10^{-4}$ . Comparing with the forecast result of NWP, RMSE of YingLong-24 for S850 relatively reduces 6.39%. This may be attributed to the sparse and un-



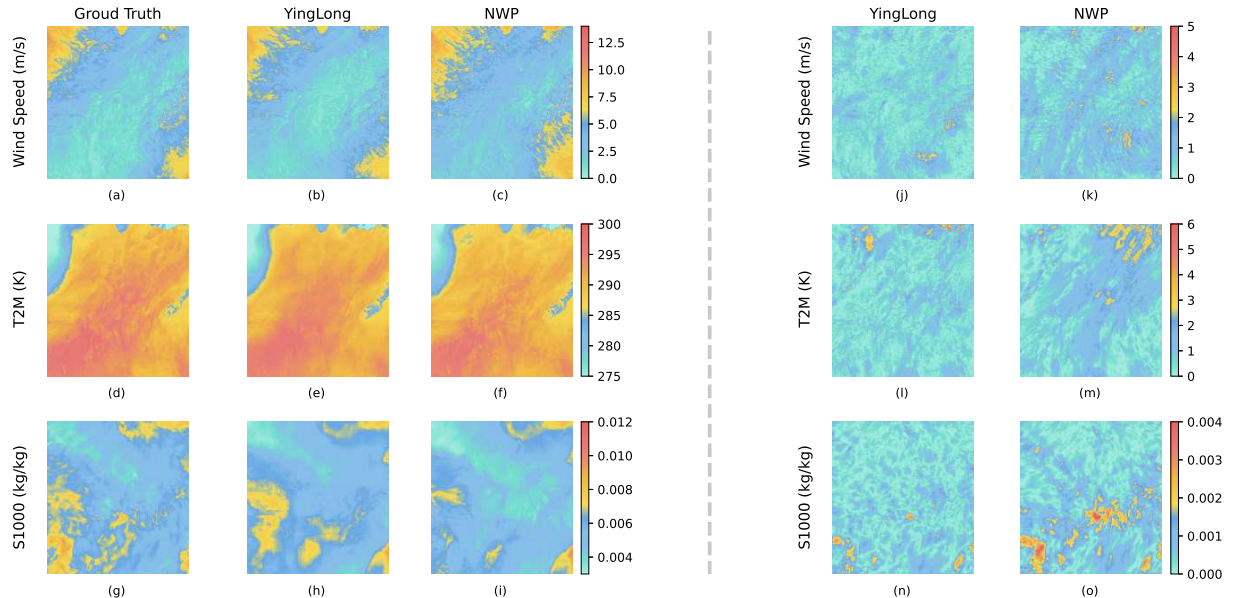


FIG. 3. Visualization for the forecasting results of YingLong. Figures (b) and (c) represent the forecasting results for 10m wind speeds (m/s) by the YingLong-12 and NWP at 10-hour forecast time, with the input time being November 10, 2022, 00:00 (UTC). The analysis data of the wind speeds at 10:00 on the same day shown in (a) can be the corresponding ground truth. In (d), the analysis data for T2M is given at 03:00 (UTC) on March 6, 2022. And (e), (f) are the corresponding forecast results for 2m T2M by YingLong and HRRR NWP at 3-hour forecast time, with input at 00:00 (UTC). For (g)-(i), the analysis data of 1000hPa specific humidity (S1000) at 05:00 on September 28, 2022 is also considered as ground truth, and YingLong and NWP at 5 hours forecast time from 00:00 (UTC) are also given. For (j)-(o), the spatial distributions of mean absolute error (MAE) for different variables are illustrated.

even selection of only 4 pressure levels for upper-level variables in the YingLong-12 model, making it difficult for the model to learn more precise relationships between variables. However, the information is sufficient for near-surface variables. The increasing information for upper-air variables in the denser 69 variables, YingLong-24 model improves the forecast performance for upper-level variables. According to the comparisons in Fig. 2, we believe that by further increasing the input of pressure levels and variables, and building up a deeper network by increasing the layers, the forecasting abilities of the YingLong model can be further improved.

Furthermore, we also compare other upper-air variables at the pressure level of 925hPa, including T925, U925, V925, and S925. Since this pressure level is outside the forecasting variables of YingLong-12, we only compare the forecasting results generated by YingLong-24 and the NWP model. According to the RMSEs and ACCs illustrated in Fig. 2 (and supplementary material Fig. 6), the forecasting results of YingLong-24 are more accurate than NWP in most cases. For instance, the forecast results of YingLong-24 for T925 are generally better than NWP results before the 9-hour forecast time. Specifically, the RMSE (in K) of NWP model at 7-hour

forecast time for T925 is 0.873, and YingLong-24 drops it to 0.815, relatively deducing 6.72%. Additionally, as we compare high-altitude variables across different pressure levels, we observe that as the pressure level decreased (actual altitude increased), the difficulty of the model's predictions gradually increased. This could be attributed to some physical changes being more extreme at high altitudes (e.g., wind speeds are often greater at high altitudes than near the surface), making it more challenging for the model to forecast such high-altitude variables due to regional boundary conditions and differences in other potential physical mechanisms.

## V. DISCUSSION

In this paper, we construct the fundamental modules of the YingLong model by parallel integrating the AFNO and Swin Transformer modules. Ingeniously, we incorporate a time encoding algorithm to endow the model with temporal information. YingLong facilitates rapid regional weather forecasting at a 3 km resolution on an hourly basis and extends its predictive capabilities up to 12 hours through rolling forecasts. If there is no nec-

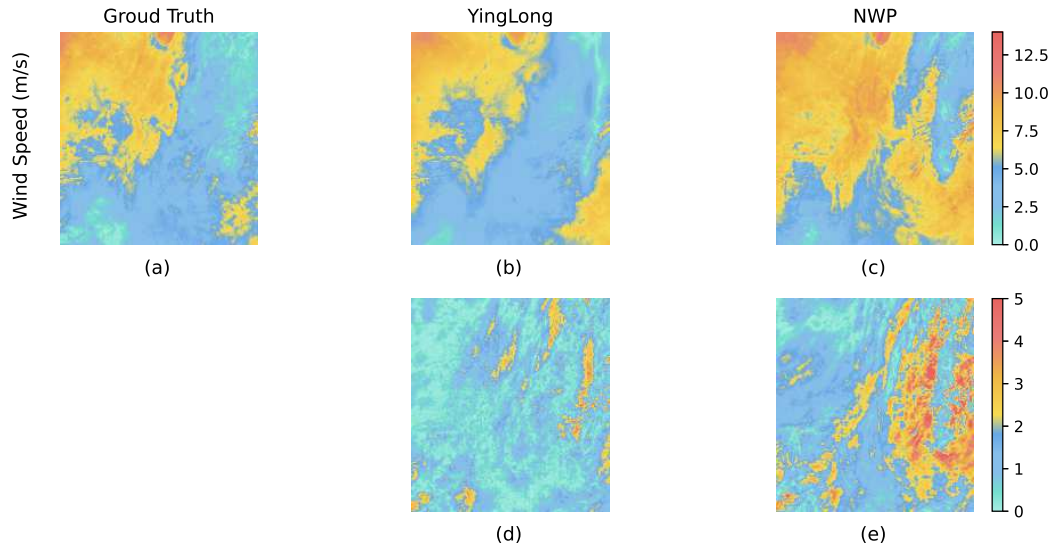


FIG. 4. Comparison of YingLong and NWP for 10m wind speed at 41h forecasting time. On November 10, 2022, at 00:00 (UTC), the YingLong model (b) and HRRR NWP (c) provided forecasted results for the 10-meter wind speed (m/s) at 17:00 (UTC) on the following day, along with comparative graphs against the analysis values in (a). Figures (d) and (e) display the spatial distributions of MAE corresponding to the forecasts from the YingLong model and NWP.

essary boundary condition for regional forecasts, YingLong would experience significant error accumulation during iterating forecasts. To address this issue, we introduce the boundary smoothing strategy, which combines the forecast results from the NWP model and YingLong around the boundary areas, significantly improving our forecasting outcomes. Relative to traditional NWP forecasts, YingLong not only outperforms in the 1-hour forecast but also maintains an advantage, even after several hours of rolling forecasts. Comparative analysis between a 12-layer YingLong with 24 variables and a 24-layer YingLong with 69 variables reveals that the former excels in near-surface forecasting, while the latter demonstrates superior performance in predicting upper-air variables. This distinction is attributed to the more detailed information provided by the 69 variables, especially in capturing intricate high-altitude variables. Our results highlight YingLong’s robust information capturing capabilities, showcasing its superior accuracy in handling certain details compared to NWP results.

Although the forecast performance for the majority of variables is impressive and exhibits clear advantages over NWP results (e.g., wind speed, specific humidity), some variables (e.g., temperature on the upper-air pressure level) do not show a sufficiently pronounced advantage in forecast outcomes. In our ongoing efforts, we intend to enhance forecast results for these variables by introducing additional auxiliary variables. We believe

that more variables and a deeper neural network can bring us much better forecasting results. Furthermore, our boundary smoothing strategy has, to a certain extent, addressed the error accumulation during the iterating forecasts. However, this approach still relies on traditional NWP forecast results. In fact, NWP can only focus on the smoothing area and offer a YingLong boundary condition, such a smoothing area is much smaller than the forecasting area we consider. Therefore, it may take less time for the NWP model to generate the forecasting results restricted to the small smoothing area.

## VI. ACKNOWLEDGMENTS

This work was supported by Major Program of National Natural Science Foundation of China (NSFC) Nos.12292980, 12292984, NSFC12031016, NSFC12201024; National Key R&D Program of China Nos.2023YFA1009000, 2023YFA1009004, 2020YFA0712203, 2020YFA0712201; Beijing Natural Science Foundation BNSF-Z210003; was funded by the Department of Science, Technology and Information of the Ministry of Education, No:8091B042240, and was also Sponsored by CCF-Baidu Open Fund CCF-BAIDU 202317.

[1] Rothfus, L. P. et al. Facets: A proposed next-generation paradigm for high-impact weather forecasting. *B. Am.*

*Meteorol. Soc.* **99**, 2025-2043 (2018).

- [2] Alley, R. B., Emanuel, K. A. & Zhang, F. Advances in weather prediction. *Science* **363**, 342-344 (2019).
- [3] Bauer, P., Thorpe, A. & Brunet, G. The quiet revolution of numerical weather prediction. *Nature* **525**, 47-55 (2015).
- [4] Molteni, F., Buizza, R., Palmer, T. N. & Petroliagis, T. The ECMWF ensemble prediction system: methodology and validation. *Q. J. Roy. Meteor. Soc.* **122**, 73-119 (1996).
- [5] Ritchie, H. et al. Implementation of the semi-Lagrangian method in a high-resolution version of the ECMWF forecast model. *Mon. Weather Rev.* **123**, 489-514 (1995).
- [6] Bauer, P. et al. *The ECMWF Scalability Programme: Progress and Plans* (European Centre for Medium Range Weather Forecasts, 2020).
- [7] Schultz, M. G. et al. Can deep learning beat numerical weather prediction? *Philos. T. R. Soc. A.* **379**, 20200097 (2021).
- [8] Balaji, V. Climbing down charney’s ladder: machine learning and the post-dennard era of computational climate science. *Philos. T. R. Soc. A.* **379**, 20200085 (2021).
- [9] Benjamin, S. G. et al. 100 years of progress in forecasting and nwp applications. *Meteorol. Monogr.* **59**, 13-1 (2019).
- [10] Allen, M. R., Kettleborough, J. & Stainforth, D. Model error in weather and climate forecasting. In *Seminar on Predictability of Weather and Climate* 279-304 (ECMWF, 2003); <https://www.ecmwf.int/en/elibrary/73407-model-error-weather>
- [11] Palmer, T. et al. Representing model uncertainty in weather and climate prediction. *Annu. Rev. Earth Pl. Sc.* **33**, 163-193 (2005).
- [12] Irrgang, C. et al. Towards neural earth system modelling by integrating artificial intelligence in earth system science. *Nat. Mach. Intell.* **3**, 667-674 (2021).
- [13] Reichstein, M. et al. Deep learning and process understanding for data-driven earth system science. *Nature* **566**, 195-204 (2019).
- [14] Rasp, S. & Thuerey, N. Data-driven medium-range weather prediction with a resnet pretrained on climate simulations: a new model for weatherbench. *J. Adv. Model. Earth Sy.* e2020MS002405 (2021).
- [15] Weyn, J. A., Durran, D. R. & Caruana, R. Improving data-driven global weather prediction using deep convolutional neural networks on a cubed sphere. *J. Adv. Model. Earth Sy.* **12**, e2020MS002109 (2020).
- [16] Rasp, S. & Thuerey, N. Purely data-driven medium-range weather forecasting achieves comparable skill to physical models at similar resolution. Preprint at <https://arxiv.org/abs/2008.08626> (2020).
- [17] Chen, G. & Wang, W. Short-term precipitation prediction for contiguous United States using deep learning. *Geophys. Res. Lett.* **49**, e2022GL097904 (2022).
- [18] Gao, Z. et al. Earthformer: exploring space-time transformers for earth system forecasting. Preprint at <https://doi.org/10.48550/arXiv.2207.05833> (2022).
- [19] Wang, Y., Long, M., Wang, J., Gao, Z. & Yu, P. S. PredRNN: recurrent neural networks for predictive learning using spatiotemporal LSTMs. In *NIPS’17: Proceedings of the 31st International Conference on Neural Information Processing Systems* 879-888 (NeurIPS, 2017).
- [20] Pathak, J. et al. FourCastNet: a global data-driven high-resolution weather model using adaptive Fourier neural operators. Preprint at <https://arxiv.org/abs/2202.11214> (2022).
- [21] Haiden, T., Janousek, M., Vitart, F., Ben-Bouallegue, Z. & Prates, F. Evaluation of ECMWF forecasts, including the 2023 upgrade. *ECMWF Technical Memoranda* (2023); <https://www.ecmwf.int/en/elibrary/81389-evaluation-ecmwf-forecasts>
- [22] Hersbach, H. et al. The ERA5 global reanalysis. *Q. J. Roy. Meteor. Soc.* **146**, 1999-2049 (2020).
- [23] Bi, K. et al. Accurate medium-range global weather forecasting with 3D neural networks. *Nature* **619**, 533-538 (2023).
- [24] Lam, R. et al. Learning skillful medium-range global weather forecasting. *Science* eadi2336 (2023)
- [25] Chen, K. FengWu: Pushing the Skillful Global Medium-range Weather Forecast beyond 10 Days Lead. Preprint at <https://arxiv.org/pdf/2304.02948.pdf> (2023).
- [26] Chen, L. et al. FuXi: a cascade machine learning forecasting system for 15-day global weather forecast. Preprint at <https://arxiv.org/pdf/2306.12873.pdf> (2023).
- [27] Nguyen, T., Brandstetter, J., Kapoor, A., Gupta, J. K. & Grover, A. Climax: a foundation model for weather and climate. Preprint at <https://arxiv.org/pdf/2301.10343.pdf> (2023).
- [28] Kain, J. S. et al. Some practical considerations regarding horizontal resolution in the first generation of operational convection-allowing NWP. *Weather. Forecast.* **23**, 931-952 (2008).
- [29] Espenholt, L. et al. Deep learning for twelve hour precipitation forecasts. *Nat. Commun.* **13**, 1-10 (2022).
- [30] Andrychowicz, M. et al. Deep learning for day forecasts from sparse observations. Preprint at <https://arxiv.org/pdf/2306.06079.pdf> (2023).
- [31] Dowell, D. C. et al. The high-resolution rapid refresh (HRRR): an hourly updating convection-allowing forecast model. part I: motivation and system description. *Weather. Forecast.* **37**, 1371-1395 (2022).
- [32] Guibas, J. et al. Efficient token mixing for transformers via adaptive fourier neural operators. *International Conference on Learning Representations (ICLR, 2021)*.
- [33] Liu, Z. et al. Swin transformer: hierarchical vision transformer using shifted windows. *International Conference on Computer Vision* 10012-10022 (IEEE, 2021).
- [34] Benjamin, S. G. et al. A north american hourly assimilation and model forecast cycle: The rapid refresh. *Mon. Weather. Rev.*, **144**(4):1669-1694, (2016).
- [35] Dosovitskiy, A. et al. An image is worth 16 × 16 words: transformers for image recognition at scale. Preprint at <https://arxiv.org/abs/2010.11929> (2020).

## Appendix A: Methods

### 1. HRRR Dataset

For training and evaluating YingLong model, we choose to utilize analysis subset of the High-Resolution Rapid Refresh (HRRR) dataset [34], which is generated through the Gridpoint Statistical Interpolation analysis system (GSI). Besides, HRRR dataset also offers the forecast results obtaining from Numerical Weather Prediction (NWP) which is generated through Advanced Research version of the Weather Research and Forecasting (WRF) Model (ARW). Both analysis and NWP results of HRRR dataset are hourly updated at 3-km grid resolution and operated by the National Oceanic and Atmospheric Administration (NOAA), covering the CONUS and Alaska, with multiple variables. Most existing deep learning weather models, such as FourCastNet, Pangu-Weather [23], GraphCast, etc. choose the ERA5 reanalysis dataset ( $0.25^\circ \times 0.25^\circ$  grid resolution) offered by European Centre for Medium-Range Weather Forecasts (ECMWF) for their input and training. In this work, we prefer to choose HRRR rather than ERA5 as our training dataset for the following reasons:

Firstly, the HRRR dataset possesses a higher spatial resolution. This implies that HRRR dataset can provide more detailed meteorological information, which is advantageous for conducting small-scale weather forecasts.

Secondly, the HRRR analysis dataset consists of assimilated data, whereas ERA5 dataset consists of reanalysis data. The reanalysis data offer the most comprehensive depiction available of past weather and climate, and they are a mixture of observations with historical short-term weather forecasts reprocessed through modern weather forecasting models. In fact, the generation of reanalysis data often experiences a certain time lag. However, in operational weather forecasting, obtaining such high-quality data as input for models is impossible. In contrast, the HRRR analysis data serves as input for the NWP of HRRR itself. Therefore, this alignment between the input of deep learning model and the input of the NWP model establishes uniformity, enabling a fairer comparison of forecast results generating by YingLong and NWP model.

We select the southeastern region of the United States as shown in Figure ??, which is around the range of 110-130E, 15-35N, with  $440 \times 408$  grid points in Lambert projection. In this work, our dataset consist of 69 variables, specifically four surface variables: mean sea level pressure (MSLP), 2m temperature (T2M), U and V component of 10m wind speed (U10 and V10, respectively), and five upper-air variables at 13 pressure levels: geopotential height (Z), specific humidity (S), temperature (T), U and V component of wind speed (U and V, respectively), and the specific pressure levels see Tabel I. And the variables

are denoted as the corresponding short name and pressure level, such as T850 represents “temperature at 850 hPa”. The training dataset ranging from 2015 to 2021, the data in 2022 for test.

### 2. Architecture

At present, many famous deep learning weather forecast models are based on the Vision Transformer (ViT) backbone [35], such as Pangu-Weather [23], FourCastNet [20], where the former one uses Shift window transformer block (Swin) [33] and the latter one uses Adaptive Fourier Neural Operator (AFNO) [32] as their core modules, respectively. In this work, since we deal with a 3-km regional grid, the large and medium spatial scales also play important roles in short term forecasting. Therefore, YingLong captures various features of variables at different scales. In order to deal with the multi-scale problem, we utilize the Window Multi-head Self-Attention (W-MSA), and Shift Window Multi-head Self-Attention (SW-MSA) blocks in Swin Transformer [33] to capture the local features of different variables. Besides, the AFNO block mainly captures the global features of the variables in the target region from the Fourier frequency space. After learning local and global features separately, the YingLong model also combines these multi-scale features together.

The YingLong model mainly consists of three components shown in Fig. 1: embedding layer, spatial mixing layers, and a linear decoder. The input data consists of  $N$  variables from Table I at time  $t$ , and forms a tensor with dimensions of  $440 \times 408 \times N$ . The lead time  $\Delta t = 1\text{h}$  in this paper. Firstly, we encode the input by the patch and position embedding layer, and then the information of time  $t$  is also adopted by the YingLong model through the time embedding layer. After fusing temporal and positional information through these two embedding layers, a  $55 \times 51 \times C$  tensor can be given. Subsequently, we use  $L$  layers of spatial mixing and multi-layer perceptrons (MLP) to capture the features at different spacial scales and the relations among various variables, respectively. Within these layers, the tensor is split according to its channel. Specifically, the partial tensor with dimension  $55 \times 51 \times (\alpha \cdot C)$  is sent to the Local branch to capture local features, and the rest of the tensor with dimension  $55 \times 51 \times ((1 - \alpha) \cdot C)$  is sent to the Global branch to capture global features. The Local and Global branches operate independently and in parallel. Then the outputs from these two branches are concatenated along the channel dimension, and a new tensor with a dimension of  $55 \times 51 \times C$  can be given. Finally, the linear decoder layer maps the extracted features, which is a tensor with dimension  $55 \times 51 \times C$  back to  $440 \times 408 \times N$ , as the predicting result of the next forecast time  $t + \Delta t$ .

**Embedding Layer.** The embedding layer in our YingLong model consists of patch embedding, position embedding, and time embedding, integrating both the spa-



tial and temporal information into the latent tensor. At first, patch embedding partitions the input tensor with a dimension of  $440 \times 408 \times N$  into 2805 patches, each patch with a size of  $8 \times 8 \times N$ . Then, through a convolutional layer, each patch is encoded into a  $C$  dimension vector, resulting in the entire input variables being encoded as a tensor of size  $2805 \times C$ . Position embedding generates 2805 learnable parameter vectors representing these 2805 relative positions, enabling the YingLong model to adaptively learn the encoding for each relative position in the region. The dimensionality of position embedding vectors is also set to  $C$ . Inspired by the Informer [? ], time embedding encodes the specific time information of input data, including year, month, day, and hour, into a  $C$  dimensional vector. Subsequently, broadcasting the time embedding vector into a  $2805 \times C$  tensor. At this point, the dimensions of the output vectors from patch embedding, position embedding, and time embedding are the same. Therefore, we can sum these vectors up, yielding the final output of the embedding layer.

**Spatial Mixing Layer.** After the embedding layer, the shape of output tensor becomes  $2805 \times C$ , it is then reshaped into a size of  $55 \times 51 \times C$ . Then the reshaped tensor is delivered to the spatial mixing layer. Subsequently, this  $55 \times 51 \times C$  tensor is split by a ratio  $\alpha$  along the channel dimension into two tensors: the one of size  $55 \times 51 \times (\alpha \cdot C)$  is delivered to the local branch, and the other of size  $55 \times 51 \times ((1 - \alpha) \cdot C)$  is sent to the global branch.

Inspired by the Swin transformer, the local branch contains only W-MSA to capture the features within the window and SW-MSA to find the relationships by shifting windows. In this work, we do not perform down-sampling, so that local branch can only focus on some detailed information on the small scale. In order to make the spatial shape of the tensor divisible by the  $8 \times 8$  window, we perform padding so that the  $55 \times 51 \times (\alpha \cdot C)$  tensor transfers to  $56 \times 56 \times (\alpha \cdot C)$ . And finally, we can get  $7 \times 7$  patches after W-MSA. Subsequently, in SW-MSA we shift the window by three patches each time. Then, after a few alternating steps of W-MSA and SW-MSA, the padding data should be removed. Therefore, a tensor with size of  $55 \times 51 \times (\alpha \cdot C)$  is returned, keeping the same size as the input tensor of the local branch.

The global branch mainly utilizes the AFNO Block. At first, we apply a 2D fast Fourier transform to the  $55 \times 51$  area along each  $(1 - \alpha) \cdot C$  channel. In the Fourier frequency domain, feature mixing is carried out by using an MLP consisting of two linear layers. Finally, using an inverse fast Fourier transform, the information from the frequency domain can then be transferred into the spatial domain.

At the end of the spatial mixing layer, we concatenate outputs from these two branches along the channel dimension to yield the final output of the spatial mixing layer, which is a  $55 \times 51 \times C$  tensor.

**Linear Decoder.** In this part, we use a simple linear layer as the decoder to map the channel dimension from

$C$  to  $(8 * 8 * N)$ . Therefore, the tensor of size  $55 \times 51 \times (8 * 8 * N)$  is reshaped back to  $440 \times 408 \times N$  as the final output of the YingLong.

We carry out experiments with two models: one with  $L = 12$  layers and the other with  $L = 24$  layers.

### 3. Training Procedure

We denote the HRRR analysis data by the tensor  $X(t)$ , where  $t$  represents the forecast time, and  $\hat{X}(t)$  and  $\hat{X}_{\text{NWP}}(t)$  denote the forecast results generated by YingLong and NWP (which is WRF-ARW) at forecast time  $t$ , respectively. We take the HRRR analysis data as input and ground truth and use an auto-regressive manner to generate predicting results for the next 12 time steps. Specifically,

$$\hat{X}(t + (i + 1)\Delta t) = \text{YingLong}(\hat{X}(t + i\Delta t)),$$

for  $i = 0, 1, \dots, 11$ , where we define  $\hat{X}(t + 0\Delta t) = X(t)$ . To reduce the accumulated errors, we use a two-step training strategy: pre-training and fine-tuning. For the pre-training step, we utilize the relative mean squared error (MSE) loss,

$$\mathcal{L}_1 = \frac{\|\hat{X}(t + \Delta t) - X(t + \Delta t)\|_2}{\|X(t + \Delta t)\|_2}.$$

And utilize Adam optimizer to train our model and update the parameters. Based on the previously pre-trained model, we begin to fine-tune our model. The loss function for the fine-tuning step is

$$\mathcal{L}_2 = \sum_{i=1}^T \frac{\|\hat{X}(t + i\Delta t) - X(t + i\Delta t)\|_2}{\|X(t + i\Delta t)\|_2},$$

where  $T = 6$ . We also use Adam optimizer to minimize the loss  $\mathcal{L}_2$ .

The model employs a cosine learning rate schedule for pre-training, starting at an initial learning rate of 0.005, iterated over 30 epochs. Following pre-training, the model is fine-tuned for 15 epochs using a cosine learning rate schedule with a lower learning rate of 0.0001. The complete training process for YingLong with 12 layers requires approximately 80 hours using 8 Nvidia V100 GPUs, and the 24-layer model requires approximately 253 hours using 8 Nvidia P40 GPUs.

### 4. Inference

In fact, the information about meteorological variables around the boundary of the forecasting region or the outside region is still important for regional forecasting. Since the weather conditions in the outside region affect

more and more on the variables within the region. Therefore, the involving of proper information around the regional boundary is quite important for the weather forecasting in the local region. Otherwise, the deep learning model should draw inferences based on little information, which is quite a heavy task for the model.

In order to provide the proper meteorological information around the regional boundary, we introduce the boundary smoothing method:

Firstly, YingLong takes the analysis variables  $X(t)$  as initial input and returns the forecasting results  $\hat{X}(t + \Delta t)$  at time  $t + \Delta t$ . On the other hand, the NWP can also give forecasting results  $\hat{X}_{\text{NWP}}(t + \Delta t)$  at time  $t + \Delta t$  with the initial condition  $X(t)$ .

Subsequently, starting from the second forecast, the output results from NWP  $\hat{X}_{\text{NWP}}(t + i\Delta t)$  for  $i \geq 1$  within the transition zone contain the boundary information of different variables. At the same time, for each point in the transition zone, YingLong can also give a result  $\hat{X}(t + i\Delta t)$ . Intuitively, as the point in the transition zone gradually moves closer to the interior zone from the outer boundary, we want the forecast results of YingLong to hold heavier weights. Therefore, for each point  $p$  in the transition zone, the above mentioned boundary smoothing progress can be formally expressed as:

$$\begin{aligned} \mathcal{X}^{(p)}(t + i\Delta t) &= \alpha^{(p)} \hat{X}^{(p)}(t + i\Delta t) \\ &\quad + (1 - \alpha^{(p)}) \hat{X}_{\text{NWP}}^{(p)}(t + i\Delta t); \\ \alpha^{(p)} &= \begin{cases} d^{(p)}/d, & d^{(p)} \leq d; \\ 0, & d^{(p)} > d \end{cases} \end{aligned}$$

where  $d^{(p)}$  denotes the shortest distance from point  $p$  in the transition zone to the interior region, and superscript “ $(p)$ ” represents the corresponding results at position  $p$ . And for each point  $q$  in the interior region,  $\mathcal{X}^{(q)}(t + i\Delta t) = \hat{X}^{(q)}(t + i\Delta t)$ .

Finally, the result  $\mathcal{X}(t + i\Delta t)$  on the whole region can then be considered as the input for the next step forecast of the YingLong model, which is

$$\hat{X}(t + (i + 1)\Delta t) = \text{YingLong}(\mathcal{X}(t + i\Delta t)).$$

Continuing such an iteration process, the forecast results for the next twelve hours can be generated. It can be found that the boundary smoothing strategy is actually kind of a combination of data-driven (YingLong model) and mechanism-driven (NWP) methods.

## 5. Evaluation Metrics

We select root mean square error (RMSE) and anomaly correlation coefficient (ACC) as the evaluation metrics for the model, which are calculated as follows:

$$\begin{aligned} \text{ACC} &= \frac{\sum_{i,j,k} (\hat{X}_{i,j,k} - \bar{X})(X_{i,j,k} - \bar{X})}{\sqrt{\sum_{i,j,k} (\hat{X}_{i,j,k} - \bar{X})^2 \sum_{i,j,k} (X_{i,j,k} - \bar{X})^2}}, \\ \text{RMSE} &= \frac{1}{N} \sum_{k=1}^N \sqrt{\frac{1}{H \times W} \sum_{i=1}^H \sum_{j=1}^W (\hat{X}_{i,j,k} - X_{i,j,k})^2}, \end{aligned} \tag{A1}$$

where  $\bar{X}$  is the climatology averaging on each variable from 2015 to 2022,  $N$  represents the number of whole test samples, and  $H$  (=440 pixels) and  $W$  (=408 pixels) are the height and width of each variable, respectively. RMSE and ACC are two important evaluation metrics widely used in various models, such as FourCastNet, Pangu-Weather, etc. Therefore, in this paper, we also mainly consider these two metrics. The higher ACC and lower RMSE stand for the better forecasting ability of the corresponding model.

## 6. Ablation experiments

In this part, we mainly discuss the necessity of boundary smoothing for the regional forecast problem. Here, we choose YingLong-12 as our research model. Fig. 5 presents partial results of the sensitivity experiment for the YingLong-12 model with or without the boundary smoothing strategy. The experiments utilize the same dataset and remain consistent in other parameter settings. Evaluation results indicate that without applying boundary smoothing, if direct rolling forecasts are conducted, although YingLong exhibits minimal deviation in the first 2 hours of forecasts, subsequent accumulation of errors occurs due to the lack of boundary information, leading to a deterioration in YingLong’s forecast performance.

After introducing the boundary smoothing scheme, during the rolling forecast, YingLong-12 not only maintains excellent forecast performance in the first 2-hour forecast time but also significantly improves its forecast results. This experiment underscores the importance of boundary conditions in regional weather forecasting, and highlights that the inclusion of a boundary smoothing strategy can substantially improve the inferencing forecast results.

## Appendix B: Data availability

The training and testing data for the YingLong model, we download a part of the HRRR dataset from <https://rapidrefresh.noaa.gov/hrrr/>, and this website can also provide the forecasting results of various variables with WRF-ARW.

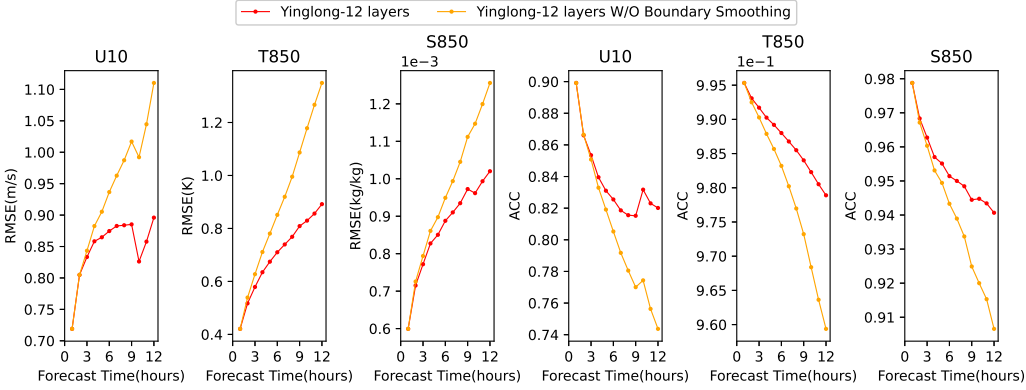


FIG. 5. Comparison of RMSE and ACC for the ablation experiment results of the boundary smoothing solution. The forecast results of YingLong-12 incorporating the boundary smoothing solution are shown in red, while the results of the direct rolling forecast are represented in orange.

**Appendix C: Code availability**

The code architecture of YingLong is developed on PaddlePaddle, a Python-based framework for deep learning, available at <https://github.com/PaddlePaddle/Paddle>. During building our architecture, we uti-

lize part of the Swin transformer, see <https://github.com/microsoft/Swin-Transformer>, the AFNO block is also involved, which can be found in <https://github.com/NVlabs/AFNO-transformer>. The trained YingLong models and some details are released in a GitHub repository: <https://github.com/PaddlePaddle/PaddleScience/tree/development>

ZZP021 H. Zhou, S. Zhang, J. Peng, S. Zhang, J. Li, H. Xiong, and W. Zhang. Informer: beyond efficient transformer for long sequence time-series forecasting. *Proceed-*

*ings of the AAAI Conference on Artificial Intelligence* **35**, 11106-11115 (2021).

Type	Full name	Abbreviation
Upper-air variables	geopotential height	Z
	specific humidity	S
	temperature	T
	U component of wind speed	U
	V component of wind speed	V
Surface variables	mean sea level pressure	MSLP
	2m temperature	T2M
	U component of 10m wind speed	U10
	V component of 10m wind speed	V10

TABLE I. We select the upper-air variables from 13 pressure levels (50 hPa, 100 hPa, 150 hPa, 200 hPa, 250 hPa, 300 hPa, 400 hPa, 500 hPa, 600 hPa, 700 hPa, 850 hPa, 925 hPa, 1000 hPa) plus the surface variables, 69 variables in total.

Index	Model	U10		V10		T2M		S1000		U850		V850		T850		S850	
		7h	12h	7h	12h	7h	12h	7h	12h	7h	12h	7h	12h	7h	12h	7h	12h
RMSE*	YingLong-12	<b>0.883</b>	<b>0.896</b>	<b>0.956</b>	<b>0.959</b>	<b>1.119</b>	<b>1.303</b>	<b>0.766</b>	<b>0.758</b>	1.810	2.016	1.800	2.027	0.740	0.892	0.910	1.020
	YingLong-24	0.897	0.919	0.972	0.981	1.121	1.385	0.773	0.767	1.688	1.916	1.724	1.934	0.694	0.818	<b>0.859</b>	<b>0.955</b>
	NWP	1.060	1.106	1.165	1.182	1.209	1.328	0.860	0.848	<b>1.687</b>	<b>1.914</b>	<b>1.685</b>	<b>1.900</b>	<b>0.674</b>	<b>0.781</b>	0.966	1.020
ACC	YingLong-12	<b>0.819</b>	<b>0.820</b>	<b>0.859</b>	<b>0.855</b>	<b>0.981</b>	<b>0.979</b>	<b>0.976</b>	<b>0.975</b>	0.934	0.919	0.944	0.920	0.987	0.979	0.950	0.941
	YingLong-24	0.811	0.809	0.856	0.850	0.981	0.974	0.975	<b>0.974</b>	<b>0.942</b>	0.927	<b>0.948</b>	0.927	<b>0.988</b>	<b>0.982</b>	<b>0.953</b>	<b>0.946</b>
	NWP	0.795	0.794	0.842	0.837	0.977	0.978	0.970	0.969	0.941	<b>0.929</b>	0.948	<b>0.929</b>	0.987	0.982	0.944	0.940

TABLE II. Comparison of the forecast results of YongLong-12, YingLong-24 and NWP at 7 hours and 12 hours.

\* In each variable, the RMSE values are provided with the corresponding units:  $U$  (m/s),  $V$  (m/s),  $T$  (K),  $S$  ( $10^{-5}$ ).

Index	Model	U925		V925		T925		S925	
		7h	12h	7h	12h	7h	12h	7h	12h
RMSE*	YingLong-24	<b>1.722</b>	<b>1.937</b>	<b>1.766</b>	<b>1.936</b>	<b>0.815</b>	0.909	<b>0.915</b>	<b>0.966</b>
	NWP	1.751	1.963	1.793	1.964	0.873	<b>0.903</b>	1.013	1.042
ACC	YingLong-24	<b>0.940</b>	0.928	<b>0.956</b>	0.931	<b>0.987</b>	0.984	<b>0.954</b>	0.953
	NWP	0.940	<b>0.931</b>	0.955	<b>0.933</b>	0.986	<b>0.986</b>	0.948	<b>0.945</b>

TABLE III. Comparison of forecast results between YingLong-24 and NWP at 7h and 12h. (This part of the result YingLong-12 is not given)

\* In each variable, the RMSE values are provided with the corresponding units:  $U$  (m/s),  $V$  (m/s),  $T$  (K),  $S$  ( $10^{-5}$ ).



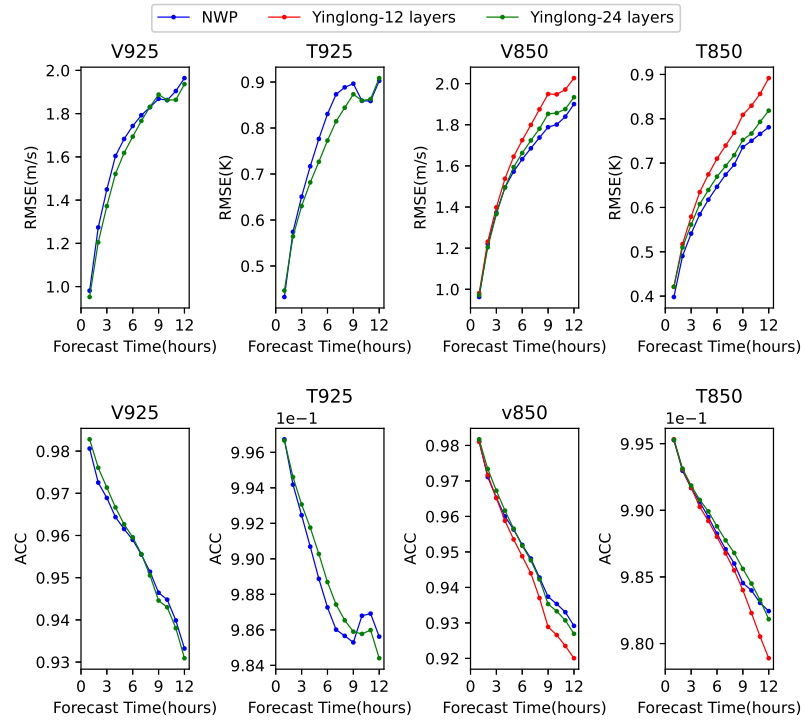
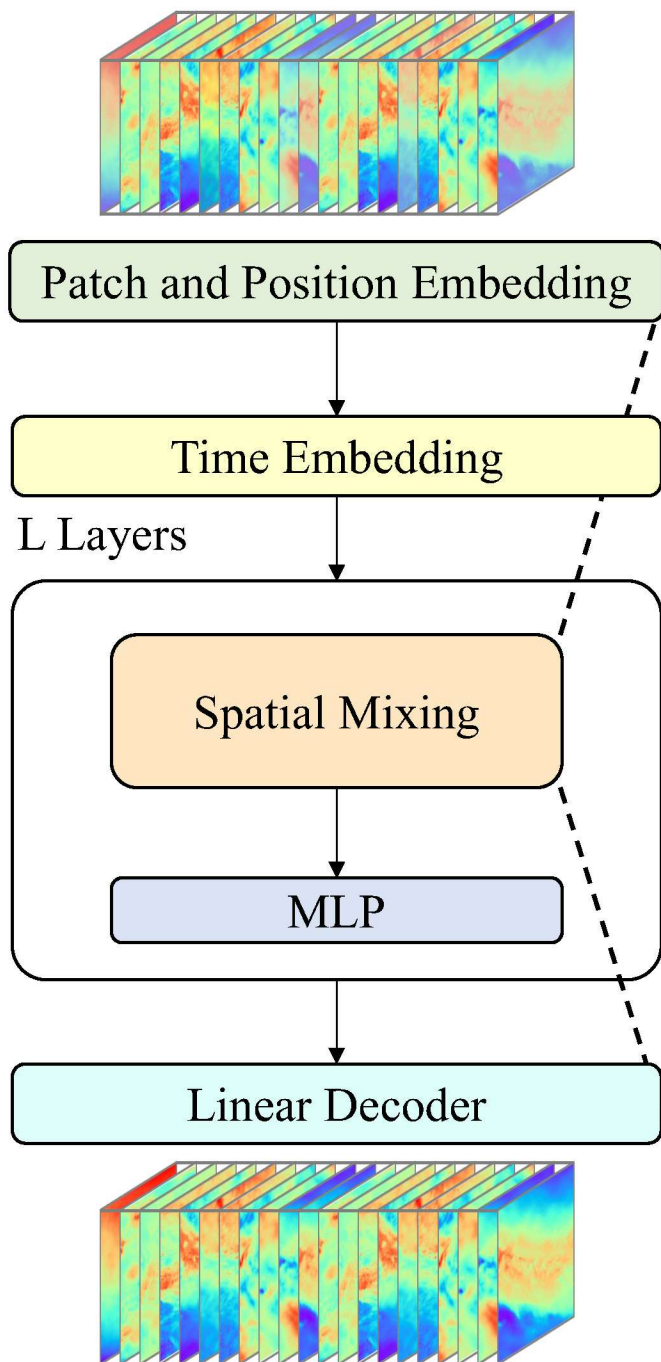
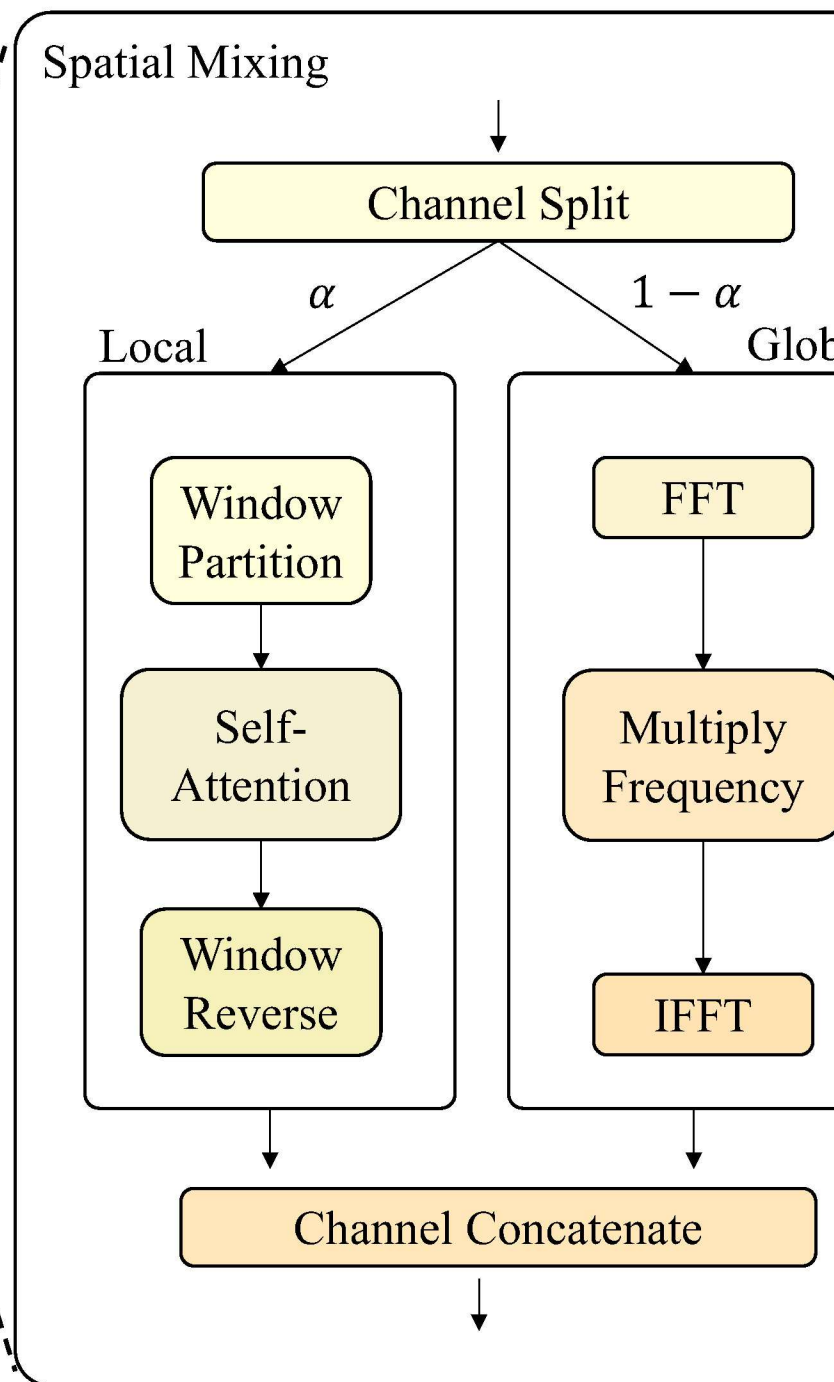


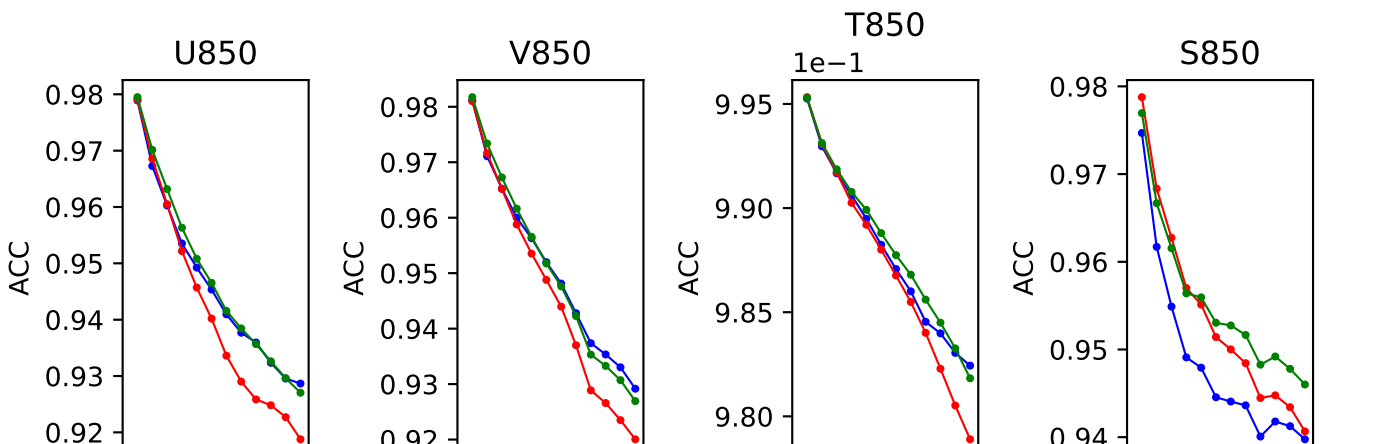
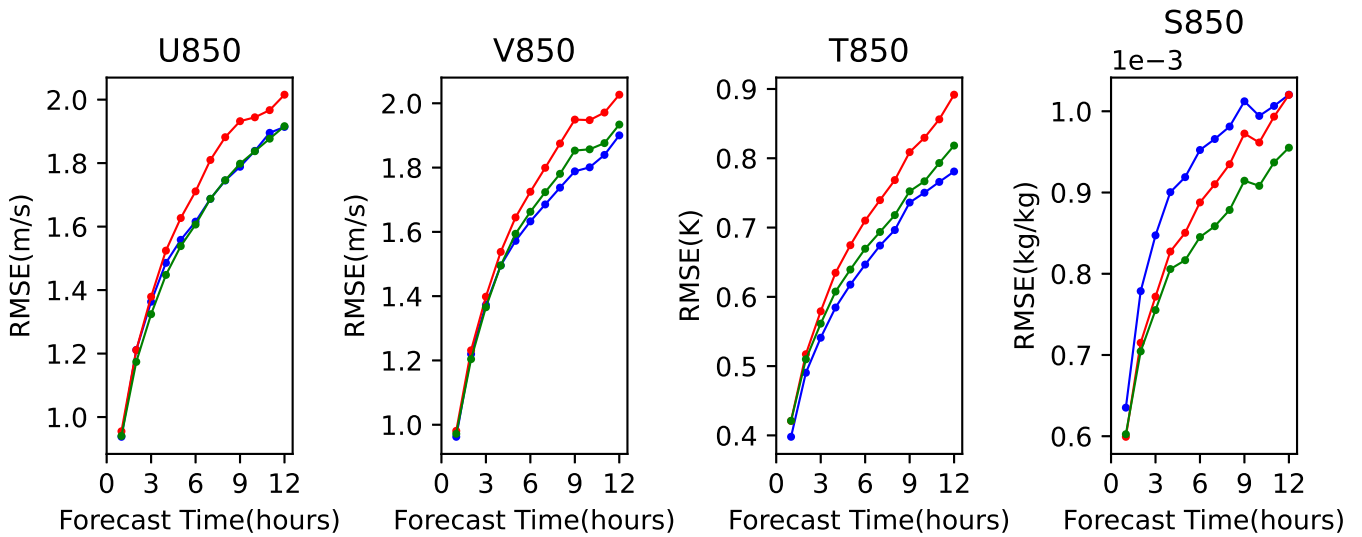
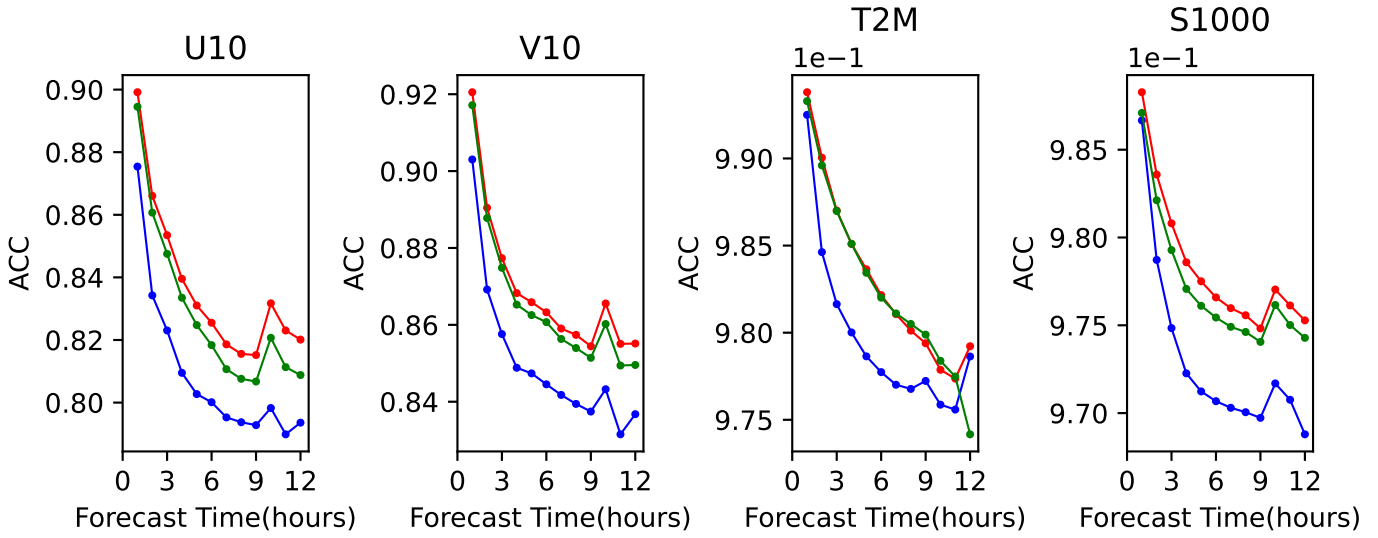
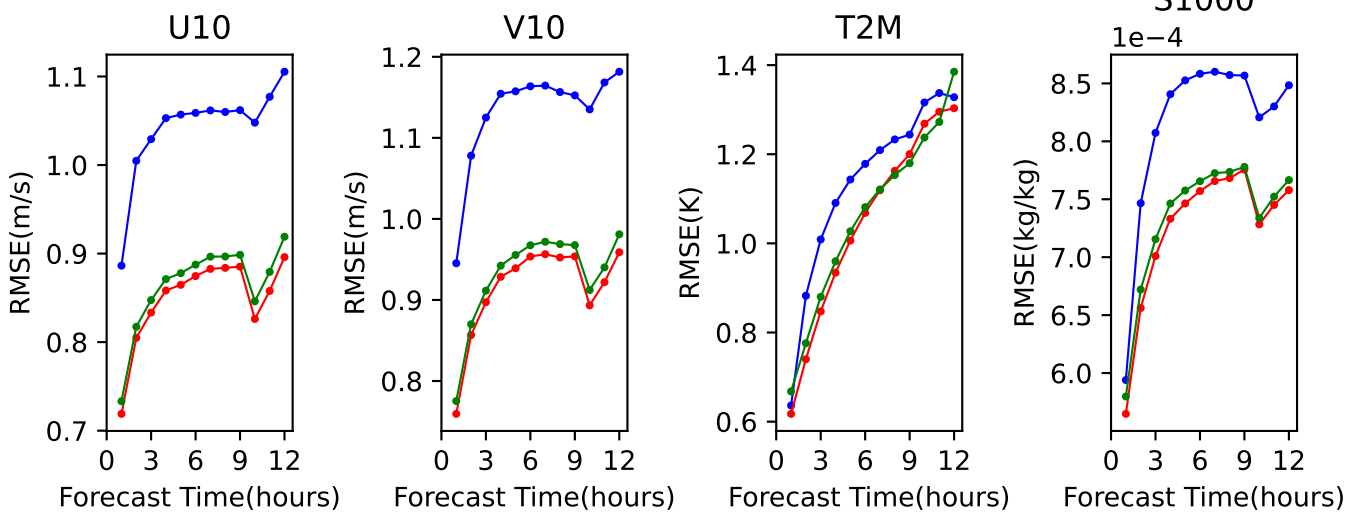
FIG. 6. The RMSEs and ACCs of the forecasting results of V925, T925, V850, T850, from YingLong-12, YingLong-24 and NWP model (i.e., WRF-ARW).

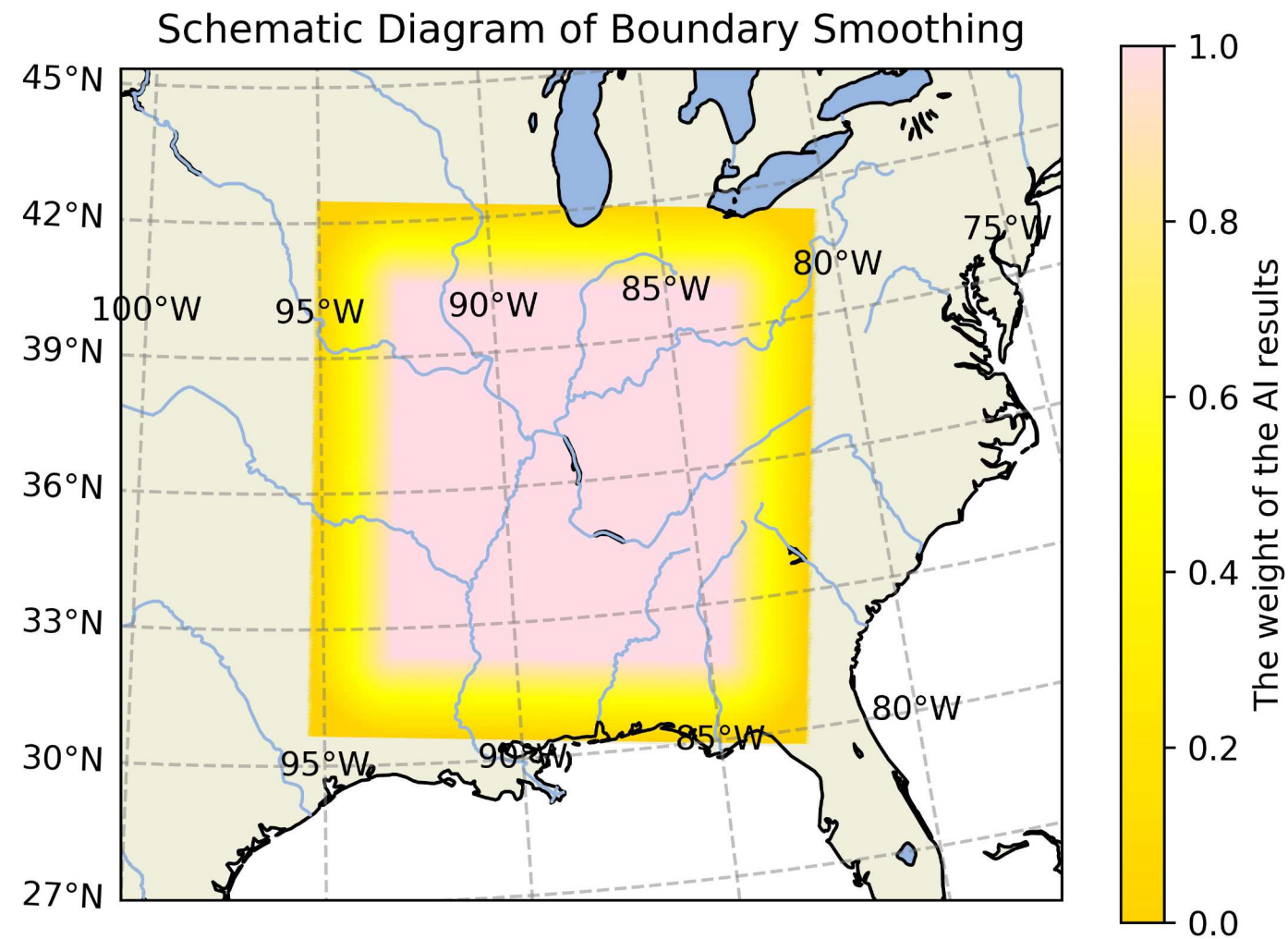


(a) Architecture

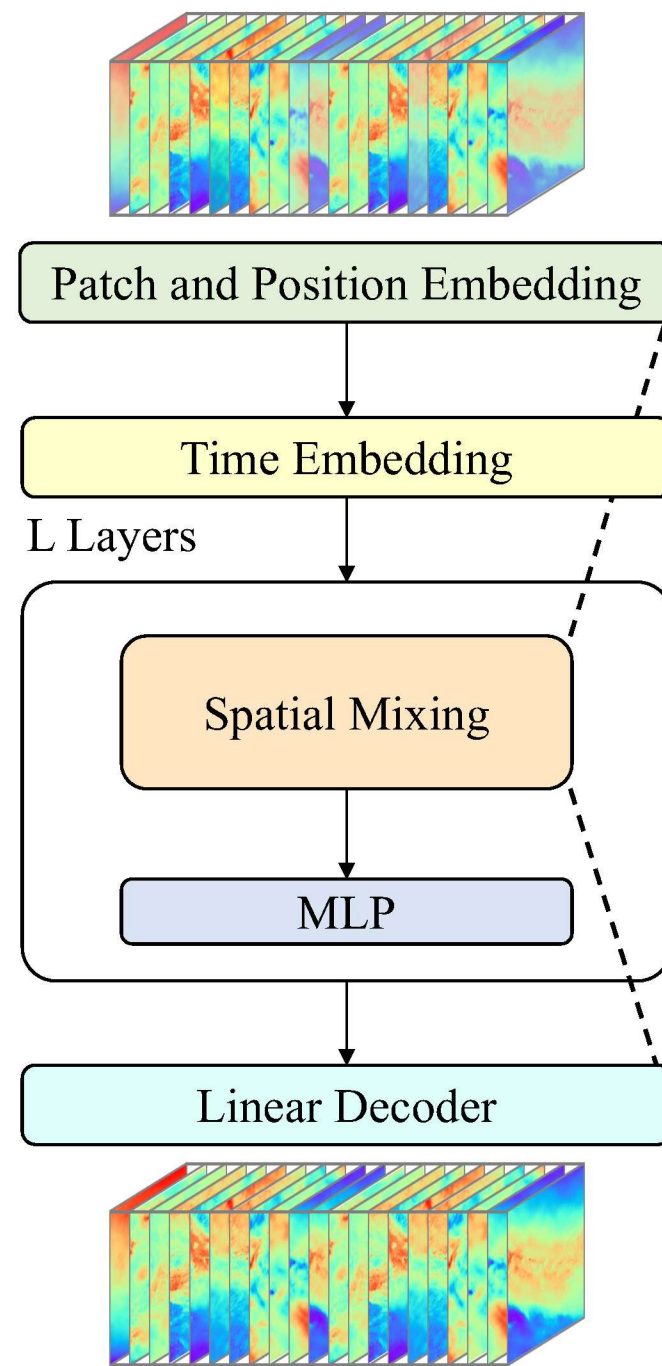


(b) Spatial Mixing

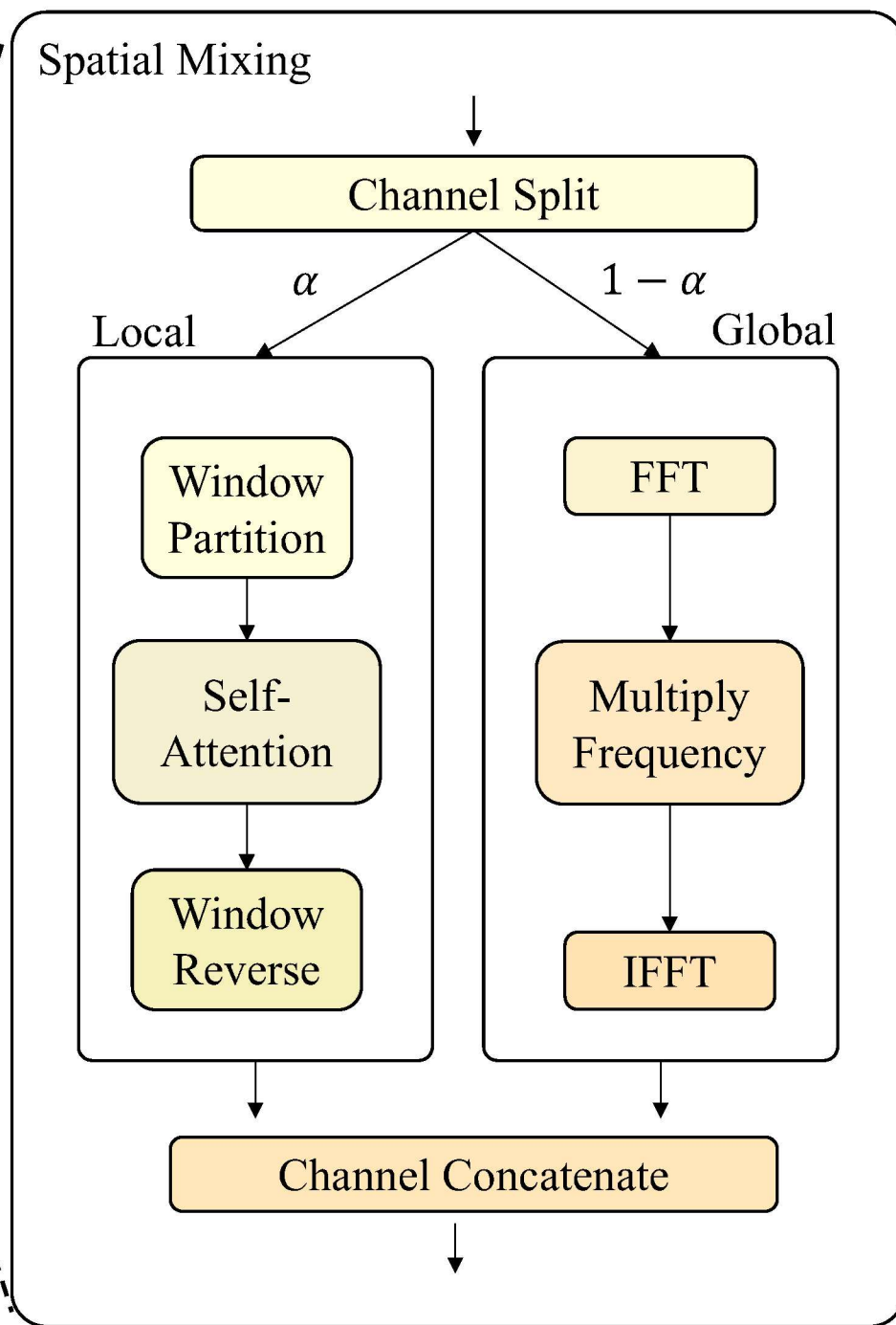




(a) Forecasting region and schematic diagram of boundary smoothing strategy



(b) Architecture



(c) Spatial Mixing



# Schematic Diagram of Boundary Smoothing

